JMEPEG (2017) 26:1283–1292
DOI: 10.1007/s11665-017-2559-0

1059-9495/$19.00

Grain Size Effect of Commercial Pure Titanium Foils on Mechanical Properties, Fracture Behaviors and Constitutive Models

Nie Daming, Lu Zhen, and Zhang Kaifeng

(Submitted June 17, 2016; in revised form February 2, 2017; published online February 21, 2017)

The constitutive models based on grain size effect are crucial for analyzing the deformation of metal foils. Previous investigations on the constitutive models concentrate on the foils whose thickness/average grain diameter (*T*/*D*) ratios are more than 3. In this study, the commercial pure titanium foils with thickness of 0.1 and 0.2 mm were employed as the experimental materials. The mechanical properties of foils with dimensions of nine different *T*/*D* ratios categorized into three ranges ($T/D < 1$, $1 \leq T/D < 3$, $T/D \geq 3$)were tested. Meanwhile, the fracture behaviors and fracture mechanisms of the samples with different *T*/*D* ratios were compared and analyzed. Besides, three constitutive models incorporating the surface layer effect and grain boundary strengthening effect were established for the three *T*/*D* ratio ranges correspondingly. In these models, the thickness of the surface layers is set T for $T/D < 1$ foils, D for $T/D > 3$, and increases with D linearly in $1 \leq T/D < 3$. The results calculated by the three models were compared. The experiments indicate that those models are all in good agreement.

Keywords constitutive model, fracture, grain size effect, micro forming

1. Introduction

Stress-strain constitutive model is a basic tool to investigate deformation behaviors and mechanical properties of metal foils. Thus, it is of significance to establish more precise constitutive models to analyze the deformation process. Compared with traditional metal sheets, metal foils with a small size in thickness would possess grain size effect during deformation (Ref 1, 2). The effect of grain size is evident in terms of mechanical properties (Ref 3, 4) and fracture behaviors (Ref 5). There are two forms of grain size effect. One of which is *the surface layer effect* (Ref 6). Grains in surface of the foil are less limited by the ambience than interior ones; hence, the flow stress of surface layer is lower. *The grain boundary strengthening effect* is another kind of grain size effect (Ref 7, 8), which is mainly attributed to the greater dislocation density, congregating impurities and lattice defects in the grain boundaries, would enhance the deformation resistance of the grain boundaries (Ref 9, 10). This effect can be described by Hall-Petch equation (Ref 11, 12) for metal sheet in ordinary sizes. However, it affects the flow stress of the foil with smaller *T*/*D* ratio more intensively.

Discussions over the constitutive models of metal foils have been reported. However, these studies mostly focus on the metal foils whose $T/D > 3$ (Ref 6, 13) and set up constitutive models ignoring the grain boundary strengthening effect for simplification. As for $T/D < 1$ foils, the constitutive model was also proposed (Ref 14). The grain boundary strengthening effect was taken into account, while both the grain interior stress (ISS) and grain boundary stress (BSS) in the surface layer are regarded to be equal to those of the interior grains (SI) of $T/D \geq 3$ foils. The model could remarkably simplify calculation, while the true result may be lower due to lack of interior grains for $T/D < 1$ foils theoretically.

In this paper, three constitutive models in three ranges of *T*/*D* ratios ($T/D < 1$, $1 \leq T/D < 3$, $T/D \geq 3$) were proposed, each of which includes *the surface layer effect*, *the grain boundary strengthening effect*, and distinguished four kinds of stress, namely ISS, BSS, grain interior stress (ISI) and grain boundary stress (BSI) in interior layer. Eight procedures were carried out in order and the four kinds of flow stress were determined in the aspect of model calculation and validation. The calculated results according to three proposed constitutive models were proved in good agreement with the experimental ones, which could be helpful for more precise evaluation of deformability of CP-Ti. In addition, the mechanical properties and their dispersion were concluded for commercial pure titanium (CP-Ti) foils belonging to 9 *T*/*D* ratios. The fracture morphology and forming mechanisms of the foils were analyzed.

2. Experimental Procedures

The experimental material adopted is CP-Ti, which contains 0.11% Fe, 0.08% Si, 0.04% C, 0.02% N, 0.015% H, 0.12% O, and the remaining proportion of Ti. The impurities (Fe, Si, etc.) would improve the strength of pure titanium. Heat treatment is taken to regulate the grain sizes of the samples. In this process, the CP-Ti foils are presumably oxidized and form white brittle oxides TiO_2 (Ref 15). The oxide layer could reduce matrix

Nie Daming, Lu Zhen, and **Zhang Kaifeng**, School of Materials Science and Engineering, Harbin Institute of Technology, Harbin, China. Contact e-mails: niedaming1989@163.com, luzhen-hit@163.com, 516075663@qq.com.

thickness and increase the flow stress in early tensile stage (Ref 16). Therefore, the samples are sealed in a quartz tube filled with argon gas (Fig. 1). Samples heated at 750 °C for 8 h with and without argon protective gas, respectively, are shown in Fig. 2. Sample surface with gas protection is almost the same as that of non-heat treated one, while that without protection appears white. The unilateral thickness of the oxide layer is approximate to 5um, accounting 10% of the foil thickness totally.

Average grain size and their standard deviation values (in form of plus/minus) after treated by nine groups of heating temperature and duration are listed in Table 1. Grain size increases pronouncedly during the 2-6 h heating duration at 750 °C. This trend is similar to that in (Ref 17). Figure 3 illustrates the microstructures of the samples with three different *T*/*D* ratios. The grain size distribution of each sample is relatively uniform (Fig. 4).

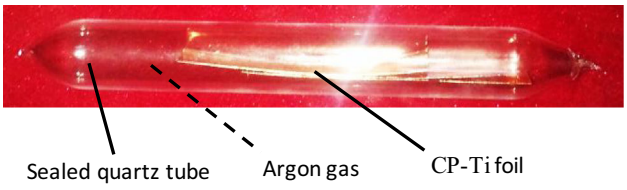

Fig. 1 CP-Ti foils in quartz tube with Ar protective atmosphere

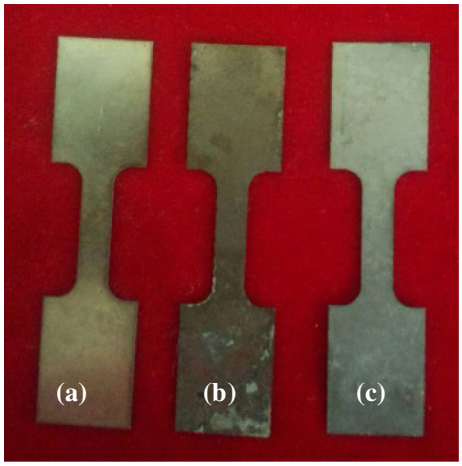

Fig. 2 Samples after different heat treatment: (a) untreated; (b) treated at 750 °C for 6 h with Ar gas protection; (c) treated 750 °C for 6 h without Ar gas protection

The Instron 5569 tensile machine is applied to complete the uniaxial tension. The SiC abrasive papers are taken to wrap the clamping faces of the foils to prevent the relative displacement between samples and clamps. The same *T*/*D* ratio samples are tested three times repetitively for reliable results. The EVO18 scanning electron microscope is adopted to observe the fracture morphology of these samples.

3. Results and Discussions

3.1 The Effect of T/D Ratio on the Mechanical Properties

The stress-strain curves of each *T*/*D* ratio sample are presented in Fig. 5. The yield strength and elongation are highest for the foils whose *T*/*D* = 11.695, while the mechanical properties turn to be the lowest when *T*/*D* = 0.722. Both the yield strength and elongation decrease with *T*/*D* ratio. Chan et al. (Ref 7) and Li et al. (Ref 18) also found the similar phenomenon. There are two responsible factors. Firstly, the fraction of surface layer increases with grain size (Ref 19) (Schematic could be seen in Fig. 9). The flow stress of surface layer is less than that in the interior grains. Hence, the total flow stress decreases with *T*/*D* ratio. Secondly, the fraction of the grain boundary decreases with *T*/*D* ratio. The deformation resistance of the grain boundary is larger (Ref 20, 21); thus, the total stress decreases.

The elongation of the foils decreases with *T*/*D* ratio. This may result from the non-uniform deformation in cross section as grain size increases. Initial intergranular crack is easier to propagate for samples with larger grains. Besides, for the foils whose $T/D < 1$, the grains in hard orientation would be difficult to rotate (Ref 22). Flow stress of the grain interior turns to be larger than that of the grain boundary; therefore, the brittle fracture occurs in grain boundary. And the elongation also decreases.

With regard to the dispersion of stress-strain curves, greatest difference lies in the three repetitive tests for *T*/*D* = 0.722 samples, while they are almost the same for *T*/*D* = 11.695 foils. The dispersion trend becomes big with decreasing *T*/*D* ratio, which could also be found in (Ref 23). The mechanism lies to the enhanced dependence of the orientation of a single grain on the total stress of sample. The grain orientation distribution is random; thus, the stress-strain curves differ even for the same *T*/*D* ratio foils with relatively fewer grains in section. However, on the other hand, all of the flow stress values tested for the *T*/*D* = 0.722 samples are less than those of the *T*/*D* = 0.799 samples, indicating the dispersion is limited to a certain extent.

Table 1 The annealing processes and results of the foils with different grain sizes

Temperature, °C	Heating duration, h	Grain size, μm	Thickness, μm	*T*/*D*
350	4	17.1 + 3.9/−10.8	200	11.695
400	4	21.3 + 4.1/−11.4	200	9.390
450	4	26.4 + 6.3/−16.6	100	3.788
550	4	42.4 + 6.6/−16.0	100	2.358
650	4	53.6 + 4.5/−20.3	100	1.866
750	2	85.8 + 5.3/−49.7	100	1.166
750	4	107.7 + 3.6/−41.2	100	0.929
750	6	128.3 + 6.8/−51.7	100	0.779
750	8	138.6 + 10.2/−77.9	100	0.722

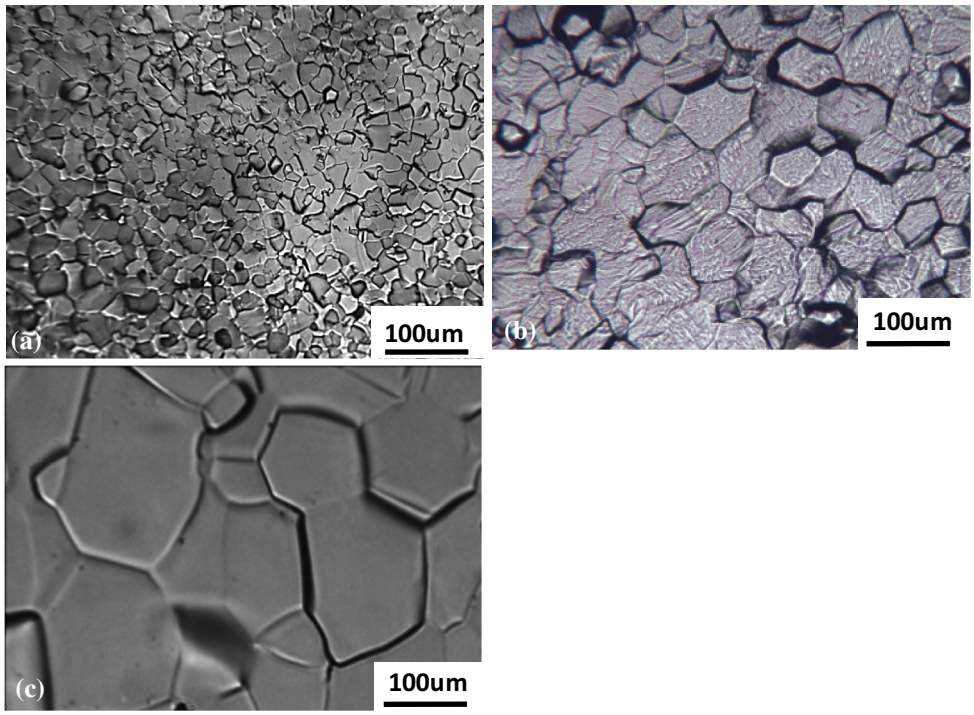

Fig. 3 Metallography of samples on different annealing conditions: (a) 400 °C for 4 h; (b) 750 °C for 2 h; (c) 750 °C for 8 h

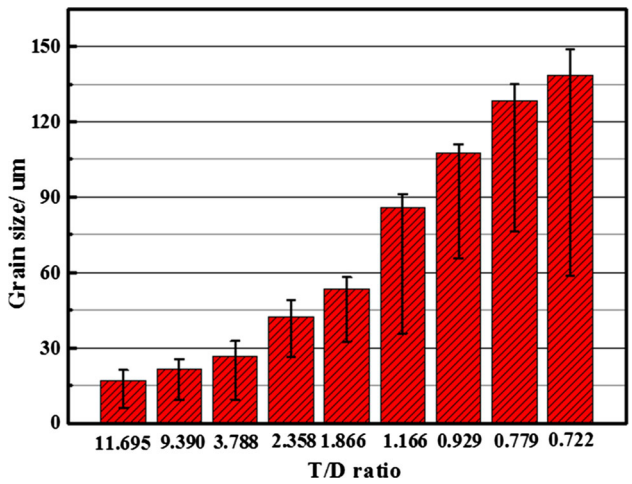

Fig. 4 The average grain size and its deviation range in each experimental group

3.2 The Effect of T/D Ratio on the Fracture Behaviors

The equiaxed dimples with different diameters distribute across the fracture surface of the CP-Ti foil whose $T/D = 3.788$ (Fig. 6a), which results from intensive dislocations slip and pile-up in necking region during tension. Cracks initiate and propagate from the micro pores, resulting in a large amount of dimples (Ref 24). The dimples indicate ductile fracture of the foils (Ref 25, 26). These findings are also found in Ti alloy (Ref 27) and pure copper (Ref 28). Dimples could also be seen in part of fracture surface of $T/D = 2.358$ sample (Fig. 6b). Moreover, the cleavage surfaces with coherent direction emerge on the edge of cross section, suggesting the cleavage planes exist there (Ref 29). The main mechanism is the different grain orientations in fracture surface. The brittle fracture may happen along the cleavage planes for the grains which are difficult to have ductile fracture. The average depth of the dimples in Fig. 6(b) is smaller than that in Fig. 6(a); Additionally, their diameters are more non-uniform, indicating the worse plasticity. $T/D = 2.358$ foil fractures in a mixed form of ductile and brittle fracture, because the co-existence of dimples and cleavage planes. Tear ridges (Ref 30) occur in Fig. 6(c), which surround the discontinuous and non-standard cleavage planes. It signals the quasi cleavage fracture (Ref 31). Secondary cracks (Ref 32) also appear, indicating the strong brittleness of this material. Figure 6(d) shows the fracture morphology of $T/D = 0.722$ foils. The large-span river pattern originates from the grain boundary and extends to the interior. Intergranular brittle fracture is presented in the lower part of the section with smooth fracture surfaces. The different grain orientation in the co-existence of cleavage fracture and intergranular brittle fracture. For the grains with river pattern, the deformation resistance is lower in grain interior than that in grain boundary, while the stress of grain interior is larger for transgranular fracture grains. This also embodies the greater dispersion in mechanical properties for foils whose $T/D < 1$.

4. Constitutive Models

Several main physical variables need to be explained first and listed in Table 2.

4.1 Constitutive Model for T/D < 1

SIS is treated equal to SII, and also SBS is thought equal to SBI in the conventional model for simplification. In this study,

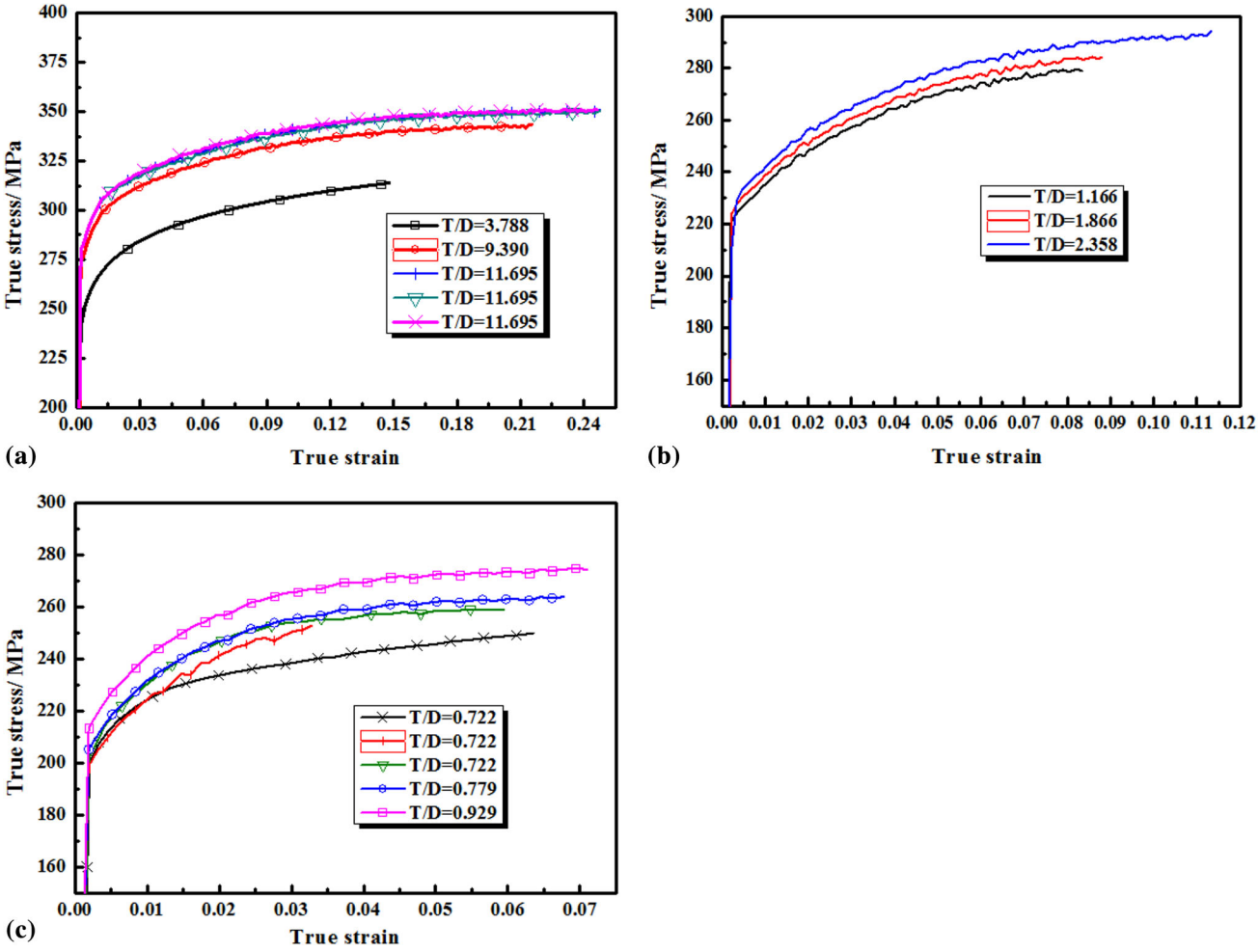

Fig. 5 Stress-strain curves of foils with different grain sizes: (a) $T/D > 3$ foils; (b) $1 < T/D < 3$ foils; (c) $T/D < 1$ foils

a novel model is proposed to distinguish the four kinds of stress. There is no whole grain in the section of $T/D < 1$ foil; thus, this section is believed as the surface layer. The schematic of grain distribution is presented in Fig. 7.

The flow stress could be expressed as:

$$\sigma = \sigma_{\text{surf}} = A_{G'_{\text{in}}}\,\sigma_{G'_{\text{in}}} + \left(1 - A_{G'_{\text{in}}}\right)\sigma_{G'_{\text{bound}}} \quad \text{(Eq 1)}$$

$$A_{G'_{\text{in}}} = \frac{1}{T}\int_{-\frac{T}{2}}^{\frac{T}{2}} \frac{\sqrt{\left(\frac{D}{2}-t\right)^2 - y^2}}{\sqrt{\left(\frac{D}{2}\right)^2 - y^2}}\,\mathrm{d}y \quad \text{(Eq 2)}$$

where, t is the thickness of grain boundary. y is the distance to the center of the grain in thickness direction. It is difficult to solve Eq 2 directly. The ''average area'' method is adopted here, and the related schematic illustration is shown in Fig. 8. S_1 is one fourth of the area of a single grain in cross section. S_2 is one fourth of the area of grain interior of a single grain in cross section. α and θ are the degree parameters.

$$S_1 = \frac{\pi D^2}{4}\cdot\frac{\alpha}{360} + \frac{1}{2}\left(\frac{D}{2}\right)\cos\alpha\cdot\left(\frac{D}{2}\right)\sin\alpha \quad \text{(Eq 3)}$$

$$\alpha = \arcsin\left(\frac{T}{D}\right) \quad \text{(Eq 4)}$$

$$S_2 = \frac{\pi(D-2t)^2}{4}\cdot\frac{\theta}{360} + \frac{1}{2}\left(\frac{D-2t}{2}\right)\cos\theta\cdot\left(\frac{D-2t}{2}\right)\sin\theta \quad \text{(Eq 5)}$$

$$\theta = \arcsin\left(\frac{T}{D-2t}\right) \quad \text{(Eq 6)}$$

Substitute Eq 3-6 to Eq 2. The result is:

$$A_{G'_{\text{in}}} = \frac{S_2}{S_1} = \frac{\frac{\pi(D-2t)^2\cdot\arcsin\left(\frac{T}{D-2t}\right)}{1440} + \frac{(D-2t)T}{8}\sqrt{1-\left(\frac{T}{D-2t}\right)^2}}{\frac{\pi D^2\cdot\arcsin\left(\frac{T}{D}\right)}{1440} + \frac{DT}{8}\sqrt{1-\left(\frac{T}{D}\right)^2}} \quad \text{(Eq 7)}$$

This result is similar to that in (Ref 14). According to the discussions in (Ref 11, 22), the relationship between t and D is:

$$t = k\sqrt{D}(k > 0) \quad \text{(Eq 8)}$$

in which the k value is 0.3 for Fe and 0.16 for Cu. The atomic number and mechanical properties of Ti are between those of Fe and Cu. Thus, the k for Ti is taken as 0.2. σ could be further solved:

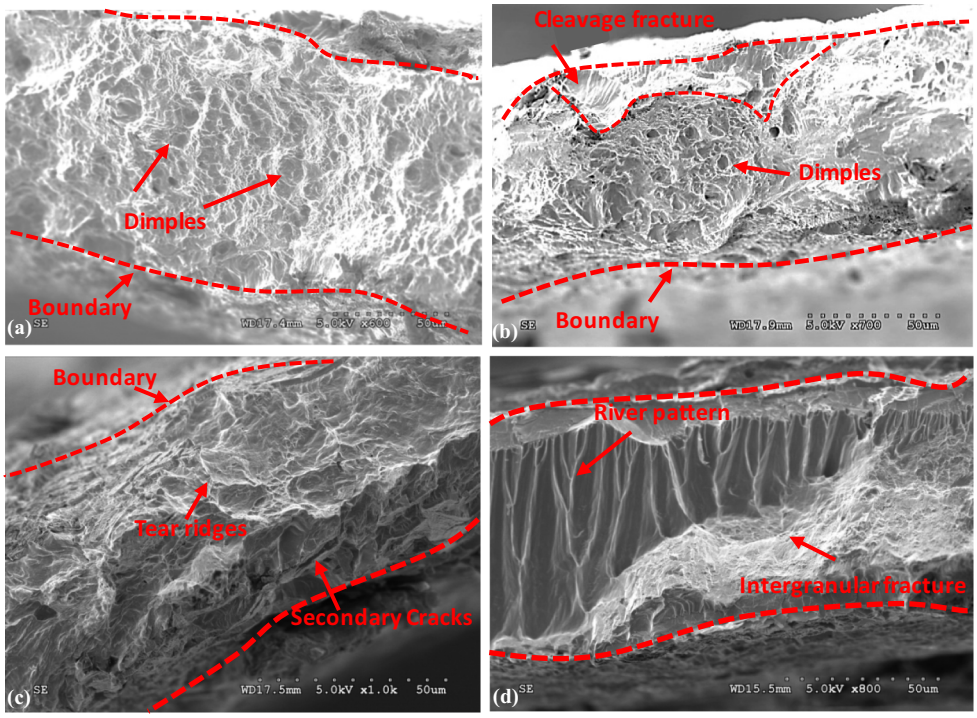

Fig. 6 Fracture morphology of CP-Ti foils with different T/D ratios after tensile fracture: (a) T/D = 3.788; (b) T/D = 2.358; (c) T/D = 1.166; (d) T/D = 0.722

$$\sigma = \sigma_{\text{surf}} = \sigma_{G'_{\text{in}}} \cdot \frac{\frac{\pi(D-2t)^2 \cdot \arcsin\left(\frac{T}{D-2t}\right)}{1440} + \frac{(D-2t)T}{8}\sqrt{1-\left(\frac{T}{D-2t}\right)^2}}{\frac{\pi D^2 \cdot \arcsin\left(\frac{T}{D}\right)}{1440} + \frac{DT}{8}\sqrt{1-\left(\frac{T}{D}\right)^2}} + \sigma_{G'_{\text{bound}}} \cdot \left\{1 - \frac{\frac{\pi(D-2t)^2 \cdot \arcsin\left(\frac{T}{D-2t}\right)}{1440} + \frac{(D-2t)T}{8}\sqrt{1-\left(\frac{T}{D-2t}\right)^2}}{\frac{\pi D^2 \cdot \arcsin\left(\frac{T}{D}\right)}{1440} + \frac{DT}{8}\sqrt{1-\left(\frac{T}{D}\right)^2}}\right\} \quad \text{(Eq 9)}$$

The parameters D, T, t are constants, $\sigma_{G'_{\text{in}}}$ and $\sigma_{G'_{\text{bound}}}$ could be determined by two T/D groups of foils. Thus, the stress flow σ could be calculated.

4.2 Constitutive Model for T/D ° 3

As for the $T/D \geq 3$ foils, the cross section includes two complete surface layers, and the interior layer possesses one layer at least in thickness direction. Therefore, the surface layer effect and grain boundary strengthening effect comprehensively function to TS. The schematic of grain distribution is illustrated in Fig. 9. TS could be written as:

$$\sigma = \eta\sigma_{\text{in}} + (1-\eta)\sigma_{\text{surf}} \quad \text{(Eq 10)}$$

$$\eta = \frac{T-2\text{D}}{T}, \quad 3\text{D} \leq T \quad \text{(Eq 11)}$$

$$\sigma_{\text{in}} = A_{G_{\text{in}}}\sigma_{G_{\text{in}}} + (1-A_{G_{\text{in}}})\sigma_{G_{\text{bound}}} \quad \text{(Eq 12)}$$

$A_{G_{\text{in}}}$ could be expressed as (Ref 24):

$$A_{G_{\text{in}}} = \frac{1}{D/2}\int_0^{\frac{D}{2}} \frac{\sqrt{\left(\frac{D}{2}-t\right)^2 - y^2}}{\sqrt{\left(\frac{D}{2}\right)^2 - y^2}}\text{d}y \quad \text{(Eq 13)}$$

According to the deduction in (Ref 21, 33), the average diameter and thickness in length direction, $\bar{D}$, $\bar{t}$, could be expressed as:

$$\bar{D} = \frac{\pi}{4}D, \quad \bar{t} = \frac{\pi}{2}t \quad \text{(Eq 14)}$$

Substitute Eq 4, 9 and 10 to Eq 8. The result is:

$$\sigma_{\text{in}} = \frac{\bar{D}-2\bar{t}}{\bar{D}}\sigma_{G_{\text{in}}} + \left(1 - \frac{\bar{D}-2\bar{t}}{\bar{D}}\right)\sigma_{G_{\text{bound}}} \quad \text{(Eq 15)}$$

The flow stress of the surface layer is:

$$\sigma_{\text{surf}} = \frac{\bar{D}-2\bar{t}}{\bar{D}}\sigma_{G'_{\text{in}}} + \left(1 - \frac{\bar{D}-2\bar{t}}{\bar{D}}\right)\sigma_{G'_{\text{bound}}} \quad \text{(Eq 16)}$$

Substitute Eq 11–16 to Eq 10. The result is:

$$\sigma = \frac{T-2\text{D}}{T}\left[\frac{D-4t}{D}\sigma_{G_{\text{in}}} + \frac{4t}{D}\sigma_{G_{\text{bound}}}\right] + \frac{2\text{D}}{T}\left[\frac{D-4t}{D}\sigma_{G'_{\text{in}}} + \frac{4t}{D}\sigma_{G'_{\text{bound}}}\right] \quad \text{(Eq 17)}$$

where $\sigma_{G'_{\text{in}}}$ and $\sigma_{G'_{\text{bound}}}$ have been solved in Eq 9, $\sigma_{G_{\text{in}}}$ and $\sigma_{G_{\text{bound}}}$ could be fitted by two groups T/D foils in this range. Thus, the flow stress model could be determined.

4.3 Constitutive Model for 1 È T/D < 3

Few researches could be found about the constitutive model of the $1 \leq \text{T/D} < 3$ foil at present. In this range, one layer of complete grains in thickness direction occupies the interior layer, while the two surface layers consist of incomplete grains. We believe that the thickness of the surface layer linearly increases with decreasing T/D. Corresponding schematic illustration is exhibited in Fig. 10. T_{surf} could be expressed as:

Table 2 Definition and abbreviated code of main physical variables

Physical variable	Definition	Abbreviated code
$\sigma_{G'_{in}}$	Flow stress of grain interior in surface layer	SIS
$\sigma_{G_{in}}$	Flow stress of grain interior in interior layer	SII
$\sigma_{G_{bound}}$	Flow stress of grain boundary in interior layer	SBI
$\sigma_{G'_{bound}}$	Flow stress of grain boundary in surface layer	SBS
σ	Total flow stress of the foil	TS
σ_{surf}	Flow stress of the surface layer	SS
σ_{in}	Flow stress of interior layer	SI
T_{surf}	Thickness of surface layer	…
$A_{G_{in}}$	Fraction of grain interior in interior layer	…
$A_{G'_{in}}$	Fraction of grain interior in surface layer	…
η	Fraction of interior layer	…
δ	Fraction of interior grains the surface layer	…
$A_{G'_{in}}1$	Fraction of grain interior in surface grains	…
$A_{G'_{in}}2$	Fraction of grain interior in partial interior grain that divided into surface layer	…
T	Thickness of grain	…
D	Diameter of grain	…
t	Thickness of grain boundary	…
$\bar{D}$	Average diameter in length direction	…
$\bar{t}$	Average thickness in length direction	…
k	Related parameter	…
x	Length direction of foil	…
y	Thickness direction of foil	…

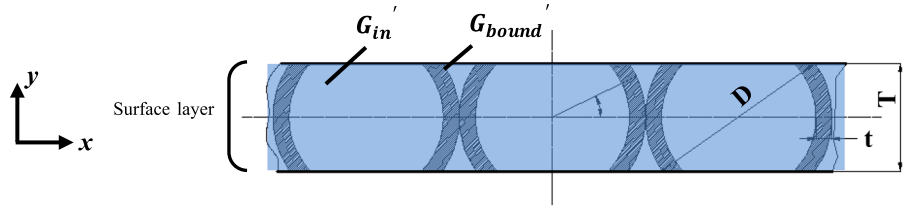

Fig. 7 Grain distribution schematic of $T/D < 1$ CP-Ti foil in cross section, x, y denotes the length and thickness direction, respectively

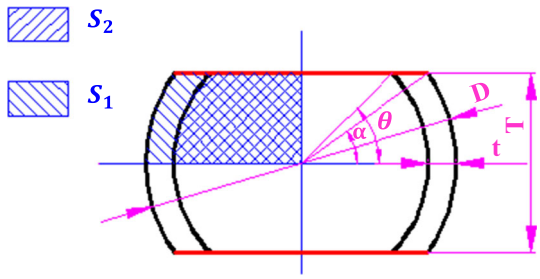

Fig. 8 Illustration of the related parameters in grain

$$T_{\text{surf}} = \frac{D}{4} + \frac{T}{4}, \quad \frac{T}{3} \le \mathrm{D} < T \tag{Eq 18}$$

$$A_{G_{\text{in}}} = \frac{\mathrm{T} - 2T_{\text{surf}}}{2} \int_0^{\frac{\mathrm{T}-2T_{\text{surf}}}{2}} \frac{\sqrt{\left(\frac{D}{2}-t\right)^2 - y^2}}{\sqrt{\left(\frac{D}{2}\right)^2 - y^2}} \mathrm{d}y \tag{Eq 19}$$

The fraction of grain interior of surface layer, $A_{G'_{\text{in}}}$, contains two parts. The first part is the fraction of grain interior in surface grains, which is marked as $A_{G'_{\text{in}}}1$. The second part is the fraction of grain interior in part of interior grain that divided into surface layer, which is marked as $A_{G'_{\text{in}}}2$.

$$A_{G'_{\text{in}}} = \delta A_{G'_{\text{in}}}1 + (1-\delta) A_{G'_{\text{in}}}2 \tag{Eq 20}$$

where δ is the fraction of interior grains in surface layer.

$$\delta = \frac{T_{\text{surf}} - \frac{T-\mathrm{D}}{2}}{T_{\text{surf}}} \tag{Eq 21}$$

$$A_{G'_{\text{in}}}1 = \left(T_{\text{surf}} - \frac{T-D}{2}\right) \int_{\left(T_{\text{surf}} - \frac{T-D}{2}\right)}^{\frac{D}{2}} \frac{\sqrt{\left(\frac{D}{2}-t\right)^2 - y^2}}{\sqrt{\left(\frac{D}{2}\right)^2 - y^2}} \mathrm{d}y \tag{Eq 22}$$

$$A_{G'_{\text{in}}}2 = \frac{T-D}{4} \int_0^{\frac{T-D}{4}} \frac{\sqrt{\left(\frac{D}{2}-t\right)^2 - y^2}}{\sqrt{\left(\frac{D}{2}\right)^2 - y^2}} \mathrm{d}y \tag{Eq 23}$$

Substitute Eq 22 and 23 to Eq 20:

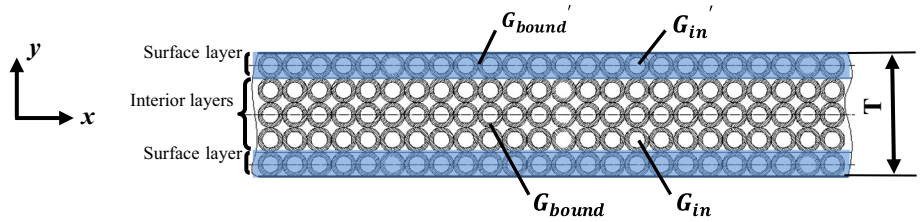

Fig. 9 Grain distribution schematic of $T/D \geq 3$ CP-Ti foil in cross section

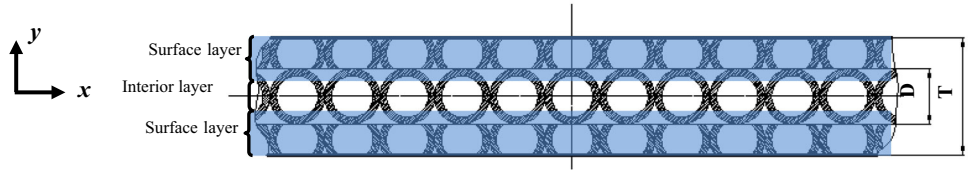

Fig. 10 Grain distribution schematic of $1 \leq T/D < 3$ CP-Ti foil in cross section

$$A_{G_{\text{in}}'} = \left(\frac{3D-\mathrm{T}}{D+T}\right)\frac{3\mathrm{D}-\mathrm{T}}{4}\int_{\frac{3\mathrm{D}-\mathrm{T}}{4}}^{\frac{D}{2}}\frac{\sqrt{\left(\frac{D}{2}-t\right)^2-y^2}}{\sqrt{\left(\frac{D}{2}\right)^2-y^2}}\mathrm{d}y + 2\left(\frac{T-D}{T+\mathrm{D}}\right)\left(\frac{T-D}{4}\right)\int_{0}^{\frac{T-D}{4}}\frac{\sqrt{\left(\frac{D}{2}-t\right)^2-y^2}}{\sqrt{\left(\frac{D}{2}\right)^2-y^2}}\mathrm{d}y \quad \text{(Eq 24)}$$

The flow stress could be expressed by Eq 12, where

$$\eta = \frac{T-2T_{\text{surf}}}{T} = \frac{T-D}{2T} \quad \text{(Eq 25)}$$

Hence, the total flow stress could be written as:

$$\begin{aligned}\sigma &= \eta\sigma_{\text{in}} + (1-\eta)\sigma_{\text{surf}} \\ &= \eta\left[A_{G_{\text{in}}}\sigma_{G_{\text{in}}} + 1 - A_{G_{\text{in}}}\sigma_{G_{\text{bound}}}\right] + (1-\eta)\left[A_{G_{\text{in}}'}\sigma_{G_{\text{in}}'} + 1 - A_{G_{\text{in}}'}\sigma_{G_{\text{bound}}'}\right] \\ &= \eta A_{G_{\text{in}}}\sigma_{G_{\text{in}}} + \eta(1-A_{G_{\text{in}}})\sigma_{G_{\text{bound}}} + (1-\eta)\left[\delta A_{G_{\text{in}}'}1 + (1-\delta)A_{G_{\text{in}}'}2\right]\sigma_{G_{\text{in}}'} \\ &\quad + (1-\eta)\left[\delta(1-A_{G_{\text{in}}'}1) + \left(1-\delta\right)(1-A_{G_{\text{in}}'}2)\right]\sigma_{G_{\text{bound}}'}\end{aligned} \quad \text{(Eq 26)}$$

η, δ, t could be calculated by inputting T and D, and the four kinds of flow stress, $\sigma_{G_{\text{in}}}$, $\sigma_{G_{\text{bound}}}$, $\sigma_{G_{\text{in}}'}$, $\sigma_{G_{\text{bound}}'}$ have been solved. Thus, the flow stress of the foil could be predicted once T and D are determined.

5. Calculation and Verification of Constitutive Models

Calculation and verification needs to be carried out in order as demonstrated in Fig. 11. In order to calculate $\sigma_{G_{\text{in}}'}$, $\sigma_{G_{\text{bound}}'}$, two groups of experimental data whose $T/D < 1$ are substituted into the constitutive model for $T/D < 1$ foils firstly (P1 in Fig. 11). The flow stress for foils with special T and D in this range thus could be predicted by the model (P2). Subsequently,

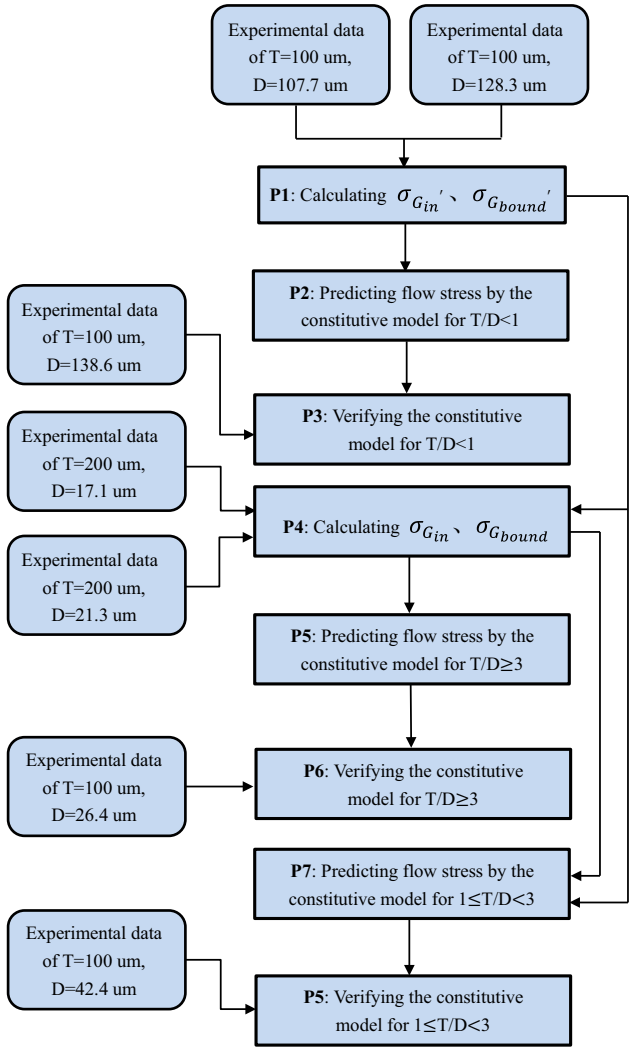

Fig. 11 Flow chart of calculation and verification of the constitutive models

the validation of the constitutive model could be carried out after comparing the calculated and experimental results (P3). The stress-strain curves of $\sigma_{G_{\text{in}}}, \sigma_{G_{\text{bound}}}$ should be fitted through the calculation of experiment values (P4) in prior to predict the flow stress for another experiment group whose $T/D \geq 3$ (P5). The prediction is based on the determination of the four kinds of flow stresses ($\sigma_{G'_{\text{in}}}$, $\sigma_{G'_{\text{bound}}}$,$\sigma_{G_{\text{in}}}, \sigma_{G_{\text{bound}}}$). The model for $T/D \geq 3$ foils could be verified then (P6). Substituting the four kinds of the flow stress into the model for $1 \leq T/D < 3$, the flow stress of the experiment group in this range could be predicted (P7) and the constitutive model could be evaluated (P8).

5.1 The Experiment Verification of the T/D < 1 Constitutive Model

The fraction of grain interior in surface layer, $A_{G'_{\text{in}}}$, could be calculated according to the Eq 7. The three groups of T and D data are substituted into the equation, and the results are listed in Table 3.

According to P1 in Fig. 11, two groups of experimental data were substituted into the model to calculate $\sigma_{G'_{\text{in}}}$, $\sigma_{G'_{\text{bound}}}$. We mark the flow stress of $T = 100$, $D = 107.7$ sample as $\sigma_{T/D=\frac{100}{107}=0.935}$, the flow stress of $T = 100$, $D = 128.3$ as $\sigma_{T/D=\frac{100}{128.3}=0.779}$. It could be obtained below:

$$\begin{cases} \sigma_{T/D=0.935} = 0.654\sigma_{G'_{\text{in}}} + 0.346\sigma_{G'_{\text{bound}}} \\ \sigma_{T/D=0.779} = 0.891\sigma_{G'_{\text{in}}} + 0.109\sigma_{G'_{\text{bound}}} \end{cases} \quad \text{(Eq 27)}$$

Which could be transformed to:

$$\begin{cases} \sigma_{G'_{\text{in}}} = 0.95\sigma_{T/D=0.779} - 0.3\sigma_{T/D=0.935} \\ \sigma_{G'_{\text{bound}}} = 3.76\sigma_{T/D=0.935} - 2.76\sigma_{T/D=0.779} \end{cases} \quad \text{(Eq 28)}$$

The stress-strain curves are presented in Fig. 12.

We could predict the flow stress of foils with another experimental group in this range according to P2 in Fig. 11. The flow stress of the foil whose $T = 100$, $D = 138.6$, could be marked as $\sigma_{T/D=\frac{100}{138.6}=0.722}$.

$$\begin{aligned} \sigma_{T/D=0.722} &= A_{G'_{\text{in}}}\sigma_{G'_{\text{in}}} + \left(1 - A_{G'_{\text{in}}}\right)\sigma_{G'_{\text{bound}}} \\ &= 0.929\sigma_{G'_{\text{in}}} + 0.071\sigma_{G'_{\text{bound}}} \end{aligned} \quad \text{(Eq 29)}$$

The results of the calculation and experiment are demonstrated in Fig. 13, where the both are in good agreement (P3).

5.2 The Experiment Verification of T/D ° 3 Constitutive Model

According to P4 in Fig. 11, the flow stress $\sigma_{G_{\text{in}}}, \sigma_{G_{\text{bound}}}$ should be determined. The two groups of stress-strain data of the foils whose $T = 200$ μm, $D = 17.1$ μm and $T = 200$ μm,

Table 3 Several parameters for the constitutive model of $T/D < 1$ foils

T	D	t	$A_{G'_{\text{in}}}$
100	107.7	2.076	0.654
100	128.3	2.265	0.891
100	138.6	2.355	0.929

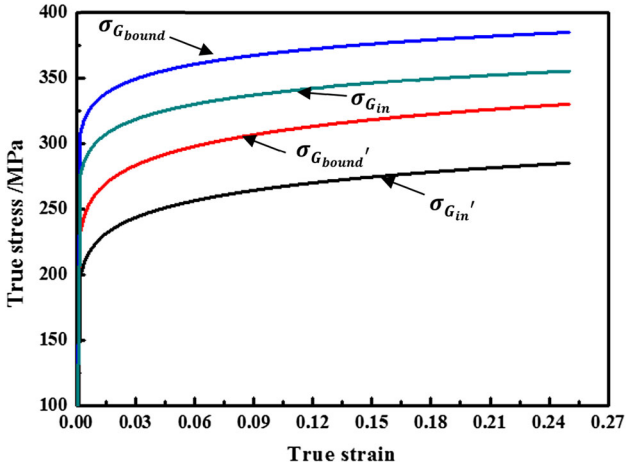

Fig. 12 Calculating results of $\sigma_{G_{\text{in}}}$, $\sigma_{G_{\text{bound}}}$, $\sigma_{G'_{\text{in}}}$, $\sigma_{G'_{\text{bound}}}$, the strains are extended to 0.25

$D = 21.3$ μm are adopted. The related parameters are calculated and listed in Table 4. According to Eq 17, it could be derived below:

$$\begin{cases} \sigma_{T/D=11.7} = 0.669\sigma_{G_{\text{in}}} + 0.16\sigma_{G_{\text{bound}}} + 0.138\sigma_{G'_{\text{in}}} + 0.033\sigma_{G'_{\text{bound}}} \\ \sigma_{T/D=9.39} = 0.653\sigma_{G_{\text{in}}} + 0.136\sigma_{G_{\text{bound}}} + 0.176\sigma_{G'_{\text{in}}} + 0.037\sigma_{G'_{\text{bound}}} \end{cases} \quad \text{(Eq 30)}$$

which could be transferred to:

$$\begin{cases} \sigma_{G_{\text{in}}} = 0.28\sigma_{G'_{\text{in}}} - 0.11\sigma_{G'_{\text{bound}}} - 10.06\sigma_{T/D=11.7} + 11.84\sigma_{T/D=9.39} \\ \sigma_{G_{\text{bound}}} = -2.04\sigma_{G'_{\text{in}}} + 0.24\sigma_{G'_{\text{bound}}} + 48.3\sigma_{T/D=11.7} - 49.48\sigma_{T/D=9.39} \end{cases} \quad \text{(Eq 31)}$$

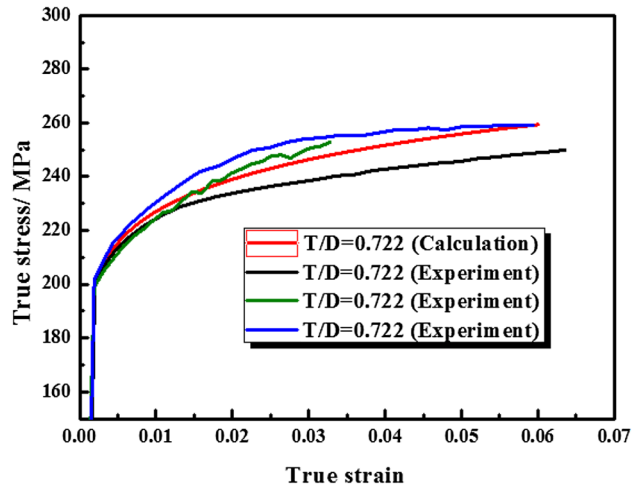

Fig. 13 Experimental and calculating results of the foils with $T = 100$ μm, $D = 138.6$ μm

Table 4 Several parameters for the constitutive model of the $T/D \geq 3$ foils

T	D	t	η	$A_{G_{\text{in}}}$
200	21.3	0.923	0.574	0.911
200	17.1	0.841	0.658	0.803

Two kinds of flow stress $\sigma_{G_{\text{in}}}, \sigma_{G_{\text{bound}}}$ are calculated and presented in Fig. 12.

According to P5 in Fig. 11, the model could be adopted to predict the flow stress now. The flow stress values in different strains of the foil whose T = 100 μm, D = 26.4 μm are calculated. The calculated results and experimental results are collected in Fig. 14, indicating both are in good agreement (P6).

5.3 The Experiment Verification of the 1 È T/D < 3 Constitutive Model

According to P7 in Fig. 11, the four kinds of flow stress, $\sigma_{G'_{\text{in}}}, \sigma_{G'_{\text{bound}}}, \sigma_{G_{\text{in}}}$ and $\sigma_{G_{\text{bound}}}$, are substituted to the constitutive model for $1 < T/D \leq 3$ foil to calculate the flow stress of the foil whose T = 100 μm, D = 42.4 μm. The related parameters

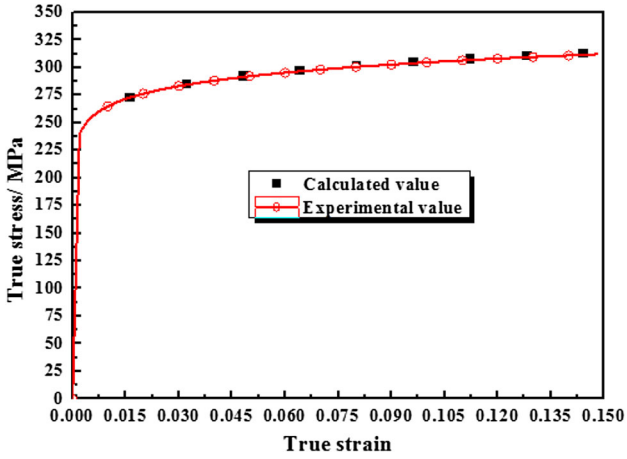

Fig. 14 The calculating and experimental results of the flow stress of the foils, T = 100 μm, D = 26.4 μm

Table 5 Several parameters for the constitutive model of the $1 < T/D \leq 3$ foils

T	D	t	η	$A_{G_{in}}$	$A_{G'_{in}}1$	$A_{G'_{in}}2$	δ
100	42.4	1.302	0.288	0.884	0.879	0.884	0.191

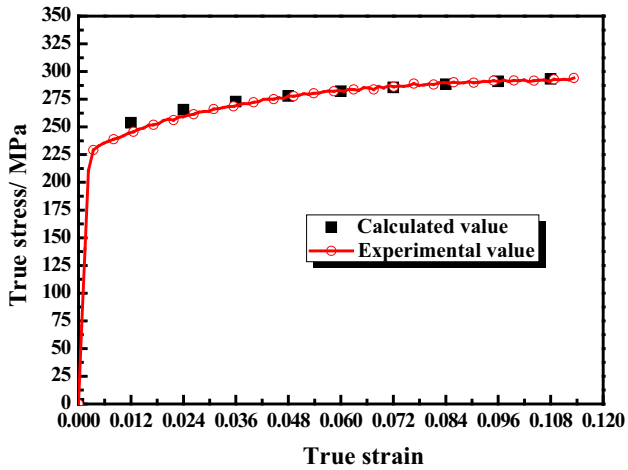

Fig. 15 The calculating and experimental results of the flow stress of the foils, T = 100 μm, D = 42.4 μm

are calculated and listed in Table 5, and both the calculation and experimental results are illustrated in Fig. 15. They are in good consistence (P8).

6. Conclusions

In this study, the foils with different T/D ratios were prepared. The mechanical properties and fracture mechanisms of the foils were tested and analyzed. Besides, the constitutive models were established for different T/D ranges, considering both surface layer effect and boundary strengthening effect. The model parameters were determined, and the predicting results are in good agreement with the corresponding experimental ones. Conclusions could be drawn as follows:

1. The flow stress and elongation of the foils decrease with T/D. Moreover, the dispersion of mechanical properties is greater as T/D decreases. The main reason is the large size and abhorrent grain orientation.
2. The fracture morphology and mechanisms are distinct in different foils. It is ductile fracture for $T/D \geq 3$ foils. For $1 \leq T/D < 3$ foils, there are mixed mode of the ductile and brittle fracture. Also the intergranular ductile fracture may occur in this range. As for $T/D < 1$ foils, the transgranular brittle fracture appears characterized by river pattern. Meanwhile, the intergranular brittle fracture emerges in part of fracture surface.
3. With regard to the constitutive model for $T/D < 1$ foils, the whole section is treated as surface layer. The boundary strengthening effect of surface layer is also taken into account. The flow stress of grain boundary, $\sigma_{G'_{\text{bound}}}$ and that of grain interior, $\sigma_{G'_{\text{in}}}$ are calculated. The calculated stress values are in good agreement with those of the experiment.
4. With regard to the constitutive model for $T/D \geq 3$ foils, the flow stress of grain boundary in interior layer, $\sigma_{G_{\text{bound}}}$, and the flow stress of grain interior layer, $\sigma_{G_{\text{in}}}$, are deduced and fitted. The flow stress of the foils in this T/D range could be predicted by the constitutive model with four important parameters, $\sigma_{G'_{\text{bound}}}, \sigma_{G'_{\text{in}}}, \sigma_{G_{\text{bound}}}, \sigma_{G_{\text{in}}}$. The calculating result is verified by experiment.
5. With regard to the constitutive model for $1 \leq T/D < 3$ foils, the thickness of surface layer increases linearly with D. The four types of flow stress $\sigma_{G'_{\text{bound}}}$, $\sigma_{G'_{\text{in}}}, \sigma_{G_{\text{bound}}}$, and $\sigma_{G_{in}}$ solved by above calculations are adopted in this model, and the prediction result in this T/D range is also agreed with the experiment.

Acknowledgment

The authors are grateful for the financial support from the National Science Foundation of China (Nos. 51675125 and 51675126).

References

1. J.T. Gau, C. Principe, and M. Yu, Springback Behavior of Brass in Micro Sheet Forming, *J. Mater. Process. Technol.*, 2007, **191**, p 7–10
2. T.A. Kals and R. Eckstein, Miniaturization in Sheet Metal Working, *J. Mater. Process. Technol.*, 2000, **103**, p 95–101

3. L. Wang, E. Mostaed, X. Cao, G. Huang, A. Fabrizi, F. Bonollo, C. Chi, and M. Vedani, Effects of Texture and Grain Size on Mechanical Properties of AZ80 Magnesium Alloys at Lower Temperatures, *Mater. Des.*, 2016, **89**, p 1–8
4. S. Chen, X. Liu, and L. Liu, Effects of Grain Size and Heterogeneity on the Mechanical Behavior of Foil Rolling, *Int. J. Mech. Sci.*, 2015, **100**, p 226–236
5. X. Ma, R. Lapovok, C. Gu, A. Molotnikov, Y. Estrin, E.V. Pereloma, C.H.J. Davies, and P.D. Hodgson, Deep drawing Behaviour of Ultrafine Grained Copper: Modelling and Experiment, *J. Mater. Sci.*, 2009, **44**, p 3807–3812
6. X. Lai, L. Peng, P. Hu, S. Lan, and J. Ni, Material Behavior Modelling in Micro/Meso-Scale Forming Process with Considering Size/Scale Effects, *Comput. Mater. Sci.*, 2008, **43**, p 1003–1009
7. W.L. Chan and M.W. Fu, Studies of the Interactive Effect of Specimen and Grain Sizes on the Plastic Deformation Behavior in Microforming, *Int. J. Adv. Manuf. Technol.*, 2012, **62**, p 989–1000
8. U.F. Kocks, The Relation Between Polycrystal Deformation and Single-Crystal Deformation, *Metall. Mater. Trans. B*, 1970, **1**, p 1121–1143
9. H. Gleiter, Nanostructured Materials: Basic Concepts and Microstructure, *Acta Mater.*, 2000, **48**, p 1–29
10. T. Eliash, M. Kazakevich, V.N. Semenov, and E. Rabkin, Nanohardness of Molybdenum in the Vicinity of Grain boundaries and Triple Junctions, *Acta Mater.*, 2008, **56**, p 5640–5652
11. W.L. Chan and M.W. Fu, Experimental Studies and Numerical Modeling of the Specimen and Grain Size Effects on the Flow Stress of Sheet Metal in Microforming, *Mater. Sci. Eng. A Struct.*, 2011, **528**, p 7674–7683
12. E.O. Hall, The Deformation and Ageing of Mild Steel: III, Discussion of Results, *Proc. Phys. Soc. B*, 2002, **643**, p 747–752
13. Q. Zheng, T. Shimizu, and M. Yang, Scale Effect on Springback Behavior of Pure Titanium Foils in Microbending at Elevated Temperature, *J. Mater. Process. Technol.*, 2016, **230**, p 233–243
14. Z. Fang, Z. Jiang, X. Wang, C. Zhou, D. Wei, and X. Liu, Grain Size Effect of Thickness/Average Grain Size on Mechanical Behaviour, Fracture Mechanism and Constitutive Model for Phosphor Bronze Foil, *Int. J. Adv. Manuf. Technol.*, 2015, **79**, p 1905–1914
15. H. Baseri and S. Sadeghian, Effects of Nanopowder TiO_2-Mixed Dielectric and Rotary Tool on EDM, *Int. J. Adv. Manuf. Technol.*, 2016, **83**, p 519–528
16. W. Zheng, X. Lin, B. Tang, and G. Wang, Experimental Investigation on Strengthening Effect of Cu_2O Film in Micro Sheet Forming of Copper, *J. Mater. Eng. Perform.*, 2016, **25**, p 1757–1762
17. H.S. Kim and W.J. Kim, Annealing Effects on the Corrosion Resistance of Ultrafine-Grained Pure Titanium, *Corros. Sci.*, 2014, **89**, p 331–337
18. L. Li, Z. Zhang, and G. Shen, Effect of Grain Size on the Tensile Deformation Mechanisms of Commercial Pure Titanium as Revealed by Acoustic Emission, *J. Mater. Eng. Perform.*, 2015, **24**, p 1975–1986
19. C.-C. Chen and C.-P. Jiang, Grain Size Effect in the Micro-V-Bending Process of Thin Metal Sheets, *Mater. Manuf. Processes*, 2011, **26**, p 78–83
20. D. Das, A. Samanta, and P.P. Chattopadhyay, Deformation Behavior of Bulk Ultrafine Grained Copper Prepared by Sub-Zero Rolling and Controlled Recrystallization, *Mater. Manuf. Processes*, 2006, **21**, p 698–702
21. M.A. Meyersm and E. Ashworth, A Model for the Effect of Grain Size on the Yield Stress of Metals, *Philos. Mag. A*, 1982, **46**, p 737–759
22. H.H. Fu, D.J. Benson, and M.A. Meyers, Analytical and Computational Description of Effect of Grain Size on Yield Stress of Metals, *Acta Mater.*, 2001, **49**, p 2567–2582
23. B. Meng and M.W. Fu, Size Effect on Deformation Behavior and Ductile fracture in Microforming of Pure Copper Sheets Considering Free Surface Roughening, *Mater. Des.*, 2015, **83**, p 400–412
24. H.K. Rafi, T.L. Starr, and B.E. Stucker, A Comparison of the Tensile, Fatigue, and Fracture Behavior of Ti-6Al-4 V and 15-5 PH Stainless Steel Parts Made by Selective Laser Melting, *Int. J. Adv. Manuf. Technol.*, 2013, **69**, p 1299–1309
25. X. Li, K. Lei, P. Song, X. Liu, F. Zhang, J. Li, and J. Chen, Strengthening of Aluminum Alloy 2219 by Thermo-Mechanical Treatment, *J. Mater. Eng. Perform.*, 2015, **24**, p 3905–3911
26. X. Li, S. Wang, S. Zhao, W. Ding, J. Chen, and G. Wu, Effect of Pulse Current on the Tensile Deformation of SUS304 Stainless Steel, *J. Mater. Eng. Perform.*, 2015, **24**, p 5065–5070
27. U. Bathini, T.S. Srivatsan, A. Patnaik, and T. Quick, A Study of the Tensile Deformation and Fracture Behavior of Commercially Pure Titanium and Titanium Alloy: Influence of Orientation and Microstructure, *J. Mater. Eng. Perform.*, 2010, **19**, p 1172–1182
28. I. Sabirov, R.Z. Valiev, I.P. Semenova, and R. Pippan, Effect of Equal Channel Angular Pressing on the Fracture Behavior of Commercially Pure Titanium, *Metall. Mater. Trans. A*, 2010, **41A**, p 727–733
29. E. Altstadt, M. Serrano, M. Houska, and A. Garcia-Junceda, Effect of anisotropic microstructure of a 12Cr-ODS steel on the fracture behaviour in the small punch test, *Mater. Sci. Eng. A Struct.*, 2016, **654**, p 309–316
30. C.W. Tan, L.Q. Li, Y.B. Chen, C.X. Mei, and W. Guo, Interfacial Microstructure and Fracture Behavior of Laser Welded-Brazed Mg Alloys to Zn-Coated Steel, *Int. J. Adv. Manuf. Technol.*, 2013, **68**, p 1179–1188
31. L. Li, Z. Zhang, and G. Shen, The Effect of Grain Size on Fatigue Crack Propagation in Commercial Pure Titanium Investigated by Acoustic Emission, *J. Mater. Eng. Perform.*, 2015, **24**, p 2720–2729
32. W. Jiang, X. Chen, B. Wang, Z. Fan, and H. Wu, Effects of Vibration Frequency on Microstructure, Mechanical Properties, and Fracture Behavior of A356 Aluminum Alloy Obtained by Expendable Pattern Shell Casting, *Int. J. Adv. Manuf. Technol.*, 2016, **83**, p 167–175
33. M.A. Meyers, A. Mishra, and D.J. Benson, The Deformation Physics of Nanocrystalline Metals: Experiments, Analysis, and Computations, *JOM*, 2006, **58**, p 41–48